Flexible Diamond Fibers for High-Energy-Density Zinc-Ion Supercapacitors

Jian, Ze; Yang, Nianjun; Vogel, Michael; Leith, Stewart; Schulte, Anna; Schönherr, Holger; Jiao, Tianpeng; Zhang, Wenjun; Müller, Julian; Butz, Benjamin; Jiang, Xin

Published in:
Advanced Energy Materials

Published: 24/11/2020

Document Version:
Final Published version, also known as Publisher's PDF, Publisher's Final version or Version of Record

Published version (DOI):
10.1002/aenm.202002202

Publication details:
Jian, Z., Yang, N., Vogel, M., Leith, S., Schulte, A., Schönherr, H., Jiao, T., Zhang, W., Müller, J., Butz, B., & Jiang, X. (2020). Flexible Diamond Fibers for High-Energy-Density Zinc-Ion Supercapacitors. *Advanced Energy Materials*, *10*(44), Article 2002202. https://doi.org/10.1002/aenm.202002202

ADVANCED ENERGY MATERIALS
www.advenergymat.de

Flexible Diamond Fibers for High-Energy-Density Zinc-Ion Supercapacitors

Ze Jian, Nianjun Yang, Michael Vogel, Stewart Leith, Anna Schulte, Holger Schönherr, Tianpeng Jiao, Wenjun Zhang, Julian Müller, Benjamin Butz, and Xin Jiang**

Supercapacitors supply high power densities but suffer from low energy densities and small specific capacitances. The design and implementation of unique capacitor electrodes are expected to overcome these challenges. Herein, flexible diamond fibers (a fibrous core/shell structure of diamond/carbon fibers) are produced through overgrowing conductive carbon fibers core with a thin boron-doped diamond film as a shell using a chemical vapor deposition technique. The resultant fibers combine the properties of boron-doped diamond with those of carbon fibers. This allows these binder-free diamond fibers to be employed as the positive electrode in the fabrication of zinc-ion supercapacitors. Together with a negative electrode fabricated from zinc nanosheet coated diamond fibers, this diamond supercapacitor delivers a high and stable specific capacitance. More importantly, it delivers high gravimetric and volumetric energy and power densities, even under severe bending states. The performance of this flexible supercapacitor is superior to previous diamond and carbon fiber-based supercapacitors. Such flexible diamond supercapacitors are promising energy storage devices for various flexible electronics.

1. Introduction

The ever-growing market of wearable and intelligent electronics has triggered continuous research into flexible energy storage devices. Taking supercapacitors (SCs) as an example,[1] fiber-based SCs are particularly promising and intriguing when compared to conventional bulky or planar SCs, owing to their unbeatable flexibility, high compatibility with the current textile industry and miniaturized device volumes and masses.[2] However, flexible SCs suffer from low specific capacitances and energy densities. Enhancing the specific capacitances and energy densities of fiber-based SCs is thus of great significance in order to facilitate their application in modern flexible electronics.[3]

The SC performance is mainly determined by the characteristics of the capacitor electrodes. The design and synthesis of novel high-performing fibrous capacitor electrodes is the resultant strategy followed to improve the specific capacitances and energy densities of fiber-based SCs. Carbon fibers (CFs) have proven to be one of the most promising capacitor electrodes due to their good conductivity, excellent flexibility, ultralight weight, and low cost. Unfortunately, CF-based SCs still exhibit low energy densities. Recently, boron-doped diamond (BDD) films, commonly deposited on nonflexible substrates (e.g., brittle Si wafers or metal substrates), have been found to be competitive SC electrodes. In clear contrast to CFs, which consist of sp^2-hybridized carbon, this sp^3-carbon material possesses a wide electrochemical potential window, long-term stability, and environmental benignity.[4] More recently, diamond paper[5] and diamond networks[4e] have been developed, which do not necessitate any supporting substrate. But these exhibited poor mechanical stability[4e,5] and partially hindered electron mobility/diffusion. To construct flexible diamond SCs with high energy density, a composite material, comprised of a sp^3 BDD coating on sp^2 CFs, is expected to provide superior properties as it combines the unique features of BDD films and CFs while simultaneously avoiding their drawbacks.

To improve the energy density of flexible SCs, another strategy that has been developed is to fabricate SC–battery hybrids. This methodology stores energy via both a reversible adsorption/desorption reaction of a capacitor-type electrode and a reversible insertion/extraction reaction of a battery-type electrode,[6] such as metal-ion hybrid capacitors.[7] Among

Z. Jian, Dr. N. Yang, Dr. M. Vogel, S. Leith, Prof. X. Jiang
Institute of Materials Engineering
University of Siegen
Paul-Bonatz Str. 9–11, Siegen 57076, Germany
E-mail: nianjun.yang@uni-siegen.de; xin.jiang@uni-siegen.de
A. Schulte, Prof. H. Schönherr
Physical Chemistry I and Research Center of Micro and Nanochemistry and Engineering (Cμ)
Department of Chemistry and Biology
University of Siegen
Adolf-Reichwein-Str. 2, Siegen 57076, Germany
T. Jiao, Prof. W. Zhang
Centre of Super-Diamond and Advanced Films (COSDAF)
Department of Materials Science and Engineering
City University of Hongkong
Tat Chee Avenue
Kowloon, Hong Kong, China
Dr. J. Müller, Prof. B. Butz
Micro- and Nanoanalytics Group
University of Siegen
Paul-Bonatz Str. 9–11
Siegen 57076, Germany
The ORCID identification number(s) for the author(s) of this article can be found under https://doi.org/10.1002/aenm.202002202.

DOI: 10.1002/aenm.202002202

these hybrid SCs, zinc-ion hybrid SCs have received significant attention,[3c,8,9] which stems from the high theoretical energy storage capacity of zinc ions (823 mAh g^{-1}) in an aqueous solution. They are also safe, have a low flammability, and are cost-effective for wearable and flexible electronics.

We are thus interested in the synthesis of novel binder-free diamond capacitor electrodes as well as their employment for the construction of SCs with high energy density. For new types of diamond capacitors, we attempt to replace the nonflexible substrates (e.g., brittle Si wafers or metal substrates) with CF. The as-fabricated diamond fibers (DFs) will be flexible and their synthetic approach will be feasible. Their surface areas will be large and their density will be low. To improve the adhesion of the BDD film on CF, an interlayer of TiC is formed between the BDD film and the CF surface. It is also beneficial to impede significant H_2 etching of the CFs during the diamond deposition process. The high conductivity and flexibility of CF combined with the intrinsic properties of BDD (e.g., wide potential window, long term stability, environmental benignity and high electrochemical activity) are expected to render the DFs to be promising capacitor electrodes for hybrid SCs. Therefore, DFs with integrated properties of CF and BDD will be applied to construct zinc-ion hybrid SC for high specific capacitance and energy densities.

Herein, DFs, a fibrous core/shell structure of diamond/carbon fibers, are designed and synthesized by means of overgrowing CFs core with a thin BDD layer as a shell by a chemical vapor deposition (CVD) process. Due to the combined features of both the BDD coating and the CF core, such DFs are the perfect capacitor electrode for the construction of flexible SCs. To further improve the energy density, a fiber-based zinc-ion hybrid SC is fabricated, consisting of the aforementioned DFs as the positive electrode and the zinc nanosheet coated DFs as the negative electrode. As confirmed by its electrical performance, i.e., its capacitance, capacitance retention, power, and energy densities, in conjunction with its extreme mechanical flexibility and excellent long-term stability, such a flexible diamond zinc-ion SC is feasible and well suited to become the high-capacity energy supplier for flexible and wearable electronics of the future.

2. Results and Discussion

The synthesized DFs are found to be highly flexible. This is shown by the lack of any obvious structural damage to the fibers following repeated bending tests (**Figure 1**A). The fibers are highly uniform (constant diameter) as indicated by field emission scanning electron microscopy (FESEM) (Figure 1B,C). In comparison to the surface of a plain CF (Figure S1A, Supporting Information), the surface of a DF is constituted by a dense polycrystalline BDD film (Figure S2, Supporting Information). The film itself is composed of homogeneous diamond grains with a grain size distribution in the range of 200 to 300 nm. To impede significant H_2 etching of the CFs and to enhance the adhesion of the BDD, a thin layer of Ti was coated on the CF surface prior to the BDD deposition. During the growth of the BDD, this results in the targeted formation of a TiC interlayer between the BDD film and the CF surface. The cross-sectional dark-field scanning transmission electron microscopy (STEM) image (Figure 1D) shows the interlayer in complete contact with the BDD film and the underlying CF. Further evidence of the good adhesion between the TiC layer and the BDD layer is given by high-resolution TEM (HRTEM) image (Figure 1F). Diamond (111) lattice planes with a lattice spacing of 0.206 nm are clearly visible in the HRTEM image. In the TiC phase, (111) lattice planes and (200) lattice planes could be resolved with lattice spacings of 0.249 and 0.216 nm, respectively. A combined fast Fourier transform (FFT) pattern, generated by summing three FFTs from different HRTEM images, is shown in Figure 1E. As marked, the rings correspond to the (111) and (200) planes of TiC as well as the (111) plane of diamond, respectively. In conclusion, the microstructural characterization demonstrates an excellent degree of crystallinity of the diamond and TiC layer. Moreover, the quality of the as-grown BDD films is significantly improved by the use of the Ti interlayer (Figure S1B, Supporting Information) when compared to those directly grown on CFs (Figure S1C, Supporting Information). The improved quality of the BDD film and the excellent flexibility of the DFs are inherited from the adhesion-promoting TiC interlayer. Furthermore, it is assumed that the TiC interlayer between the CF substrate and the BDD film decreases the ohmic resistance between the BDD film and the CF substrate. It is beneficial for charge transport at the substrate interface and therefore the charge transfer resistance between the electrolytes and DFs is reduced.[10]

To compare the electrochemical performance of DFs with different grain sizes, three DFs (DF-1, DF-2, and DF-3) were systematically prepared by applying different deposition parameters (Table S1, Supporting Information). The thickness of the as-grown BDD layers was between 200 to 250 nm (Figure S2, Supporting Information). The FESEM images of these DFs indicate an increase in the grain sizes of the as-grown BDD layers from tens of nanometers to the range of 200–300 nm due to the changes to the deposition parameters (Figure S3, Supporting Information). X-ray diffraction (XRD) confirms the crystal structure (Figure 1G). The XRD patterns of pure CFs show only one broad diffraction peak centered at 26.4°, corresponding to the typical graphite structure with nanosized domains within the CFs. The XRD patterns of all synthesized DFs include pronounced additional peaks at 43.9° and 75.3°, corresponding to the (111) and (220) planes of diamond, respectively. The peaks at 35.9° and 41.7° are ascribed to the (111) and (200) planes of cubic TiC, respectively. These results are in excellent agreement with the TEM analyses and further verify the formation of the TiC interlayer. Note here, no Ti peaks were observed, indicating full carbonization of the Ti thin film during the process of BDD deposition within the detection limits of XRD. This is due to the fast diffusion of carbon into the deposited Ti under the conditions used for diamond deposition.[4c,11]

Raman spectroscopy (Figure 1H) was employed to further confirm the diamond crystal structure of the DFs. The peak at 1330 cm^{-1} is assigned to sp^3-carbon of the BDD layer.[12] The broad and intense G-band at around 1620 cm^{-1} is attributed to the CFs. The X-ray photoelectron spectra (XPS) survey spectrum of DFs (Figure S4, Supporting Information) reveals the presence of only carbon and oxygen elements. Moreover, no further signals attributed to Ti or other elements are detected.

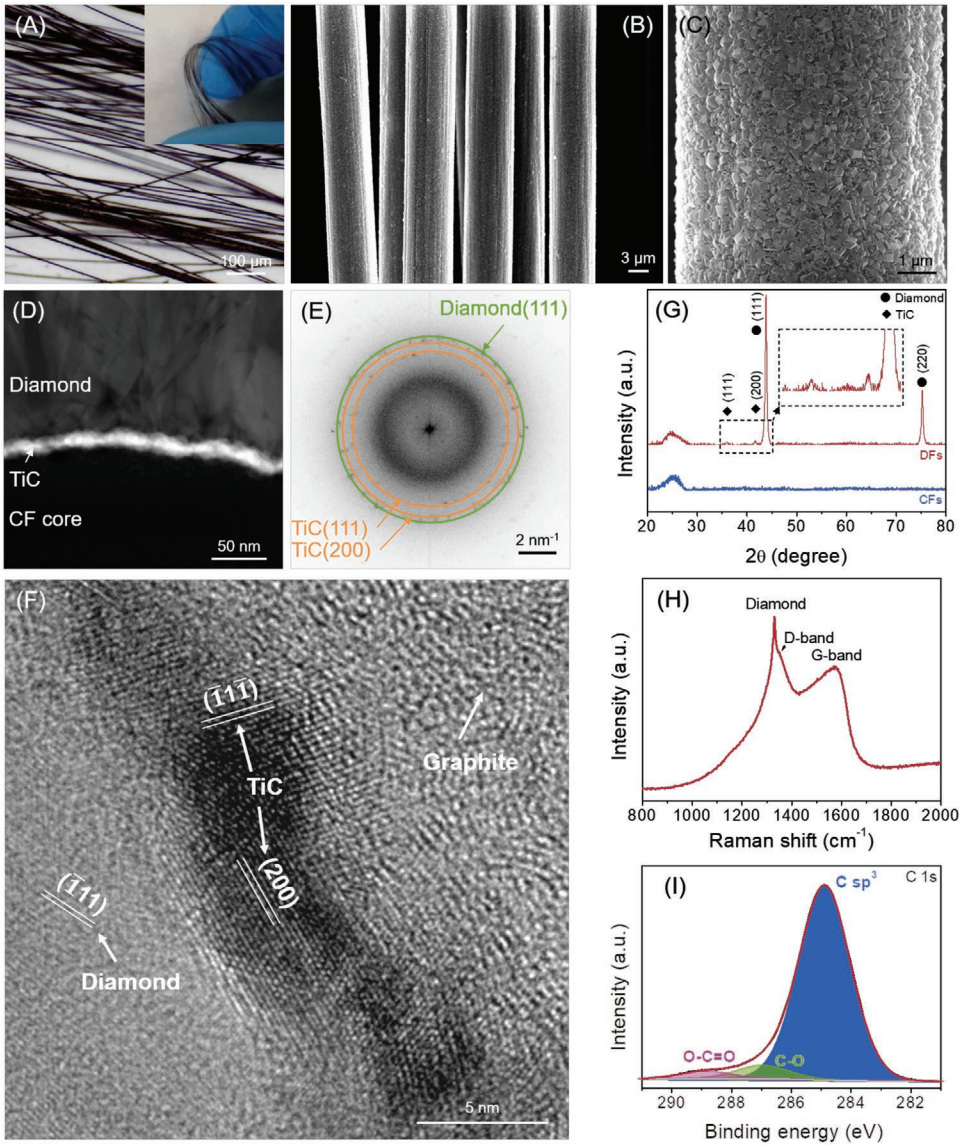

Figure 1. Characterizations of DFs: A) Optical micrograph with an inset digital photograph. B,C) FESEM images (secondary electron mode), D) dark-field STEM image: the TiC appears brightest, while crystallographic contrast is seen in the polycrystalline BDD film, E) FFT of HRTEM images (like in (F)), F) representative HRTEM closeup of the TiC interlayer, G) XRD spectra of DFs and CFs, H) Raman spectrum, and I) high-resolution C 1s XPS spectra (The black line is experimental curve and the red line is fitted curve. The colored areas represent the individual components).

Therefore, it can be concluded that the underlying CF surface is covered by a dense and homogeneous BDD film, which is thicker than 10 nm. In the high-resolution C 1s XPS spectrum (Figure 1I), the peak at a binding energy of 285.0 eV is assigned to sp^3-carbon of the diamond component.[13] The two peaks at binding energies of 286.5 and 288.3 eV are associated with carbon present in oxygen-containing chemical groups of hydroxyl (C—OH)/ether (C—O—C) and carbonyl (O—C=O) respectively.[14] As the fabricated DFs combine the unique features of a BDD film and CFs, which are the strongly reduced charge transfer resistance between electrolyte and the BDD paired with high mechanical flexibility and fatigue resistance, they are outperforming building blocks for flexible electrodes. Secondary ion mass spectroscopy (SIMS) measurements were further employed to confirm the homogeneity of doped boron atoms in the BDD film (Figure S5, Supporting Information). Compared with an undoped diamond film, the distribution of boron atoms in the BDD film is homogeneous throughout the whole BDD film.

The as-grown DFs possess low wettability in water, due to the characteristics of the hydrogen-termination found in the as-grown BDD film. Consequently, the DFs were treated by an O_2 plasma prior to their application as a capacitor electrode resulting in an oxygen-terminated surface for strongly improved wettability.[4] The dramatic difference in water contact angles on untreated and plasma-treated surfaces is depicted in Figure S6 in the Supporting Information. Such treated DFs were utilized as capacitor electrodes for the SC assembly. A

bunch of DFs was used as the positive electrode, while another bunch of DFs coated with zinc nanosheets was used for the negative electrode. The zinc nanosheets were directly deposited in the SC cell by in situ electrodeposition, which makes any additional synthesis/electrodeposition step redundant prior to the assembly of the SC cells. The color of the negative electrode (zinc nanosheet coated DFs) is gray, while that of the positive electrode (uncoated DFs) is black. The FESEM images in Figure S7A,B in the Supporting Information shows that the deposited zinc nanosheets are homogeneously and vertically aligned on the surface of the DFs. Such a 3D nanostructure with enlarged surface area offers a favorable pathway for the transfer of electrons/ions and is beneficial for the diffusion of electrolytes. The XRD patterns of the as-prepared zinc nanosheets show a crystalline phase of zinc metal (Figure S7C, Supporting Information), revealing their high degree of crystallinity. Here, the zinc nanosheets were deposited onto the negative electrode, oxygen evolution occurred at the positive electrode. During this process, abundant oxidizing functional groups were electrogenerated.[15] These oxidizing functional groups offered a pseudocapacitance for the as-fabricated zinc-ion SCs.[16]

Prior to evaluating the performance of the as-fabricated zinc-ion SCs, the capacitances of the positive electrodes (treated DFs) were studied in 1.0 M $ZnSO_4$ aqueous solution using a three-electrode configuration. The cyclic voltammograms (CVs) were recorded within a potential range of 0–1.0 V at a scan rate of 50 mV s^{-1} (Figure S8A, Supporting Information). For comparison, CVs of a CF electrode and other DFs (with different diamond grain sizes) were recorded under identical conditions as well. All CVs exhibit stable rectangular shapes, indicating ideal electrical double-layer capacitor (EDLC) behavior. At the same scan rate and within the same potential range, the integrated charges (namely the areas of the CVs) of all three DFs are larger than that of CFs demonstrating the larger capacitances of DFs compared to CFs. Of these DF samples, sample DF-3, which features a diamond grain size of 200–300 nm, exhibits the highest capacitance. The interfacial resistances were estimated based on the Nyquist plots of these electrodes (Figure S8B, Supporting Information), which were recorded at their open-circuit potentials in 1.0 M $ZnSO_4$ aqueous solution. Sample DF-3 shows a reduced interfacial resistance, which is much closer to that of CFs. This suggests the apparent enhancement of interfacial charge–carrier transfer on the surface of DF-3. Consequently, DF-3 was selected as the capacitor electrode in the construction of the zinc-ion SCs.

The capacitive behavior of the electrodes constructed from sample DF-3 and the CF sample was investigated and compared using a 1.0 M Na_2SO_4 aqueous solution (Figure S9A, Supporting Information) and a 1.0 M Na_2SO_4 aqueous solution containing 0.05 M $[Fe(CN)_6]^{3-/4-}$ (Figure S9B, Supporting Information). The Nyquist plots were obtained in 1.0 M Na_2SO_4 aqueous solution containing 0.05 M $[Fe(CN)_6]^{3-/4-}$ (Figure S9C, Supporting Information). The equivalent circuit diagram was fitted[17] using the equivalent circuit, consisting of an ohmic resistor of the cell components (R_e), a resistor of the surface film (R_{sf}), a charge–transfer resistor at the interface between electrode and electrolyte (R_{ct}), constant phase elements of the surface film (CPE_{sf}) and a double layer (CPE_{dl}) and a Warburg impedance of bulk ion diffusion (W). Judging from the capacitances and R_{ct} values, one can conclude that DFs feature outstanding capacitive behavior and are promising for the construction of either EDLCs or pseudocapacitors.

The fiber-based zinc-ion SCs were constructed using DFs as the positive electrode and zinc nanosheet coated DFs as the negative electrode. Their performance was evaluated in 1.0 M $ZnSO_4$ aqueous solution. The scanned potential range from 0.2 to 1.8 V was selected to prevent both oxygen as well as hydrogen evolution within this operation range.[7c,16] As control experiment, the performance of SCs fabricated using CFs as electrodes (CFs and Zn nanosheet coated CFs as negative and positive electrodes) was evaluated as well. Figure S10A,B in the Supporting Information shows the arising CVs at a scan rate of 50 mV s^{-1} and the galvanostatic charging/discharging (GCD) curves at a charging/discharging current density of 200 mA g^{-1}, respectively. The integrated areas of CVs of the SCs using DFs as the capacitor electrodes (DF-SC) are much larger than those from the SC using CFs as the capacitor electrodes (CF-SC). Consequently, the zinc-ion DF-SC has better capacitive behavior than CF-SC. The same results were obtained from the comparison of their GCD curves. The calculated capacitance of the zinc-ion DF-SC is 35.1 F g^{-1} at a current density of 200 mA g^{-1}, which is 14-fold higher than CF-SC (2.5 F g^{-1}).

The performance of the zinc-ion DF-SC was further evaluated in 1.0 M $ZnSO_4$ aqueous solution with different scan rates and charging/discharging current densities. **Figure 2**A presents the CVs at different scan rates. These CVs exhibit a gradual deviation from the ideal rectangular shape, which is significantly different from the rectangular shape of a typical EDLC. This behavior originates from the energy storage mechanism of the Zn-ion SC. In the zinc-ion DF-SC, the zinc coated DFs provide a battery-type capacitance, stemming from the quasi-reversible deposition/stripping process of zinc ions. This primary faradaic reaction leads to the appearance of one pair of peaks in the acquired CVs. On the other hand, the oxidizing functional groups on the surface of the DFs interact with the zinc ions, resulting in a pseudocapacitance at the positive electrode of the Zn-ion SC.[6c,8a,15,18] The related GCD curves recorded at different current densities are presented in Figure 2B. The acquired GCD curves are asymmetrical. More apparently, the discharging times are longer than the corresponding charging times at low current densities. It is known that BDD provides active sites for oxygen reduction in oxygen containing electrolytes.[15,19] Namely, additional reactions (e.g., oxygen reduction) might be involved during the discharging process. In our case, the used electrolyte actually contained oxygen, which was generated during the process of in situ coating of the DFs with zinc nanosheets. The GCD curves of the zinc-ion DF-SC were then evaluated in 1.0 M $ZnSO_4$ aqueous solution before and after the removal of the generated oxygen (Figure S11, Supporting Information). After the removal of the dissolved oxygen, the recorded GCD curve is nearly symmetrical, i.e., the charging time is almost equal to the discharging time. Therefore, oxygen reduction contributed to the additional discharging capacitances of the zinc-ion DF-SC in an oxygen-containing electrolyte, especially at low current densities. Consequently, the zinc-ion DF-SC is a hybrid ion capacitor, exhibiting different energy storage mechanisms. Firstly, the zinc nanosheet-coated DFs provide a battery-type capacitance to the device. Secondly, the oxidizing functional groups on the surface

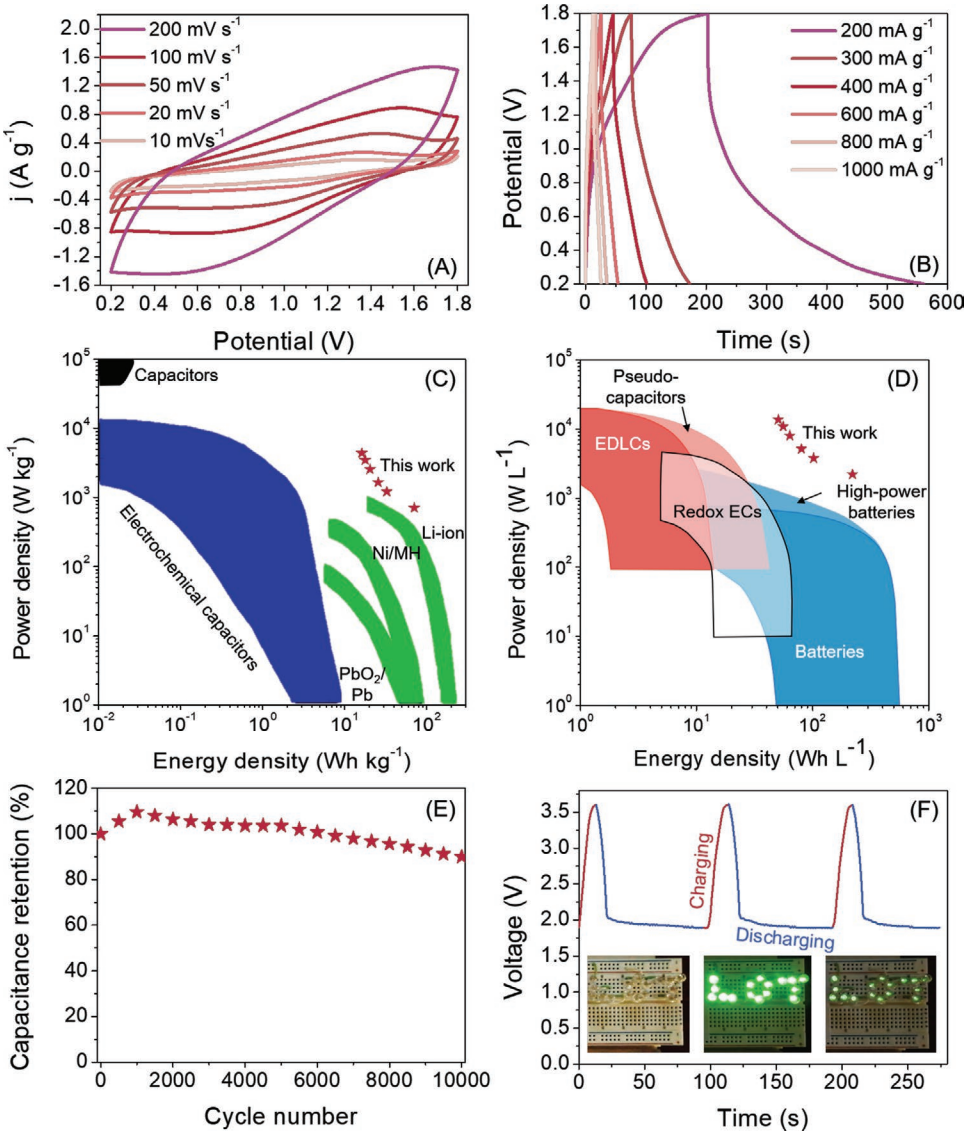

Figure 2. Performance of a zinc-ion SC in 1.0 M $ZnSO_4$: A) CVs at different scan rates, B) GCD curves at different current densities. Comparison of Ragone plots of this SC with other SCs, batteries and capacitors in C) gravimetric units[21a] and D) volumetric units,[21b] E) cycling stability at a current density of 1 A g^{-1}, F) typical voltage–time curves during the charging/discharging processes. The inset photographs show the LOT array of 16 LEDs, which lighted up during the process.

of the DFs offer a pseudocapacitance. Furthermore, the oxygen reduction reaction on the DFs contributes an additional discharging capacitance to the zinc-ion DF-SC. Based on the combined mass of the two capacitor electrodes (only 1.6 mg), the calculated capacitances of this zinc-ion SC are 35.1, 16.3, 12.7, 10.1, 8.9, and 8.1 F g^{-1} at the current densities of 200, 300, 400, 600, 800, and 1000 mA g^{-1}, respectively. Note here that this cylinder DF has a surface area of 3068.48 cm^2 g^{-1}, which is much larger than a planar BDD electrode and other BDD micro/nanostructures. If the mass of the active electrode materials is used, the calculated gravimetric specific capacitances are 246.1, 114.3, 89.1, 70.8, 62.4, and 56.8 F g^{-1} at the current densities of 200, 300, 400, 600, 800, and 1000 mA g^{-1}, respectively. These values are significantly higher than those reported for diamond and CF based SCs so far.[4b,d,e,20]

Such a hybrid system is expected to feature both a high power plus a high energy density. The energy and power densities of the zinc-ion DF-SC were calculated using the GCD curves at various current densities. This SC delivers an energy density of 70.7 Wh kg^{-1} at a power density of 709.0 W kg^{-1}. Even at a power density as high as 4395.3 W kg^{-1}, the energy density of this SC still remains at 16.2 Wh kg^{-1}. With a power density of 4395.3 W kg^{-1}, a full charging/discharging process is completed within 25.7 s. Moreover, these energy density and power density values are significantly higher than those of diamond and CF based SCs so far (Figure S12, Supporting Information).[4b,d,e,20] The Ragone plots of other commercial energy storage systems (e.g., typical SCs, modern rechargeable batteries and capacitors) are further summarized. The mass and volume of capacitor electrodes from these systems are used during the calculation

processes.[21] Clearly, this diamond zinc-ion SC features a higher gravimetric (Figure 2C) and volumetric (Figure 2D) energy and power densities than other energy storage devices. Therefore, it is a promising energy storage system for portable device applications.

The cycling stability of this zinc-ion SC was further evaluated by means of the GCD technique. During a long-time charging/discharging process (e.g., after 10 000 cycles) and at a high charging/discharging current density (e.g., 1 A g^{-1}), the SC retains about 89.9% of its initial capacitance (Figure 2E). Electrochemical impedance spectroscopy (EIS) measurements of this zinc-ion DF-SC during the charging/discharging cycles were conducted. The corresponding Nyquist plots (Figure S13, Supporting Information) are composed of arcs in the high-medium frequency regions and inclined lines in the low frequency areas. During the initial 500 charging/discharging cycles, the interfacial resistance is decreased, because the concomitant cyclic variation of the surface wetting properties of the DFs enhances the pseudocapacitance of this zinc-ion DF-SC during these cycles. Meanwhile, the intermediates generated on the DFs (e.g., •OH) promote the interaction of zinc ions with the oxidizing functional groups on the surface of the DFs, leading again to the enhanced pseudocapacitance. The interfacial resistance starts increasing from the 1000th charging/discharging cycle, indicating an increased barrier to the interfacial charge transport. In this regard, the morphology and the composition of two electrodes of this zinc-ion DF-SC after 10 000 charging/discharging cycles were further examined by means of SEM, XRD, and energy-dispersive X-ray spectroscopy (EDX). The negative electrode still exhibits a dendrite-free morphology (Figure S14A, Supporting Information), although minor shape and size changes of these nanosheets are noticed. No byproducts were detected after such a cycling test (Figure S14C, Supporting Information). The EDX results show that the atomic percentage of Zn is slightly reduced (Table S3, Supporting Information), indicating the minor loss of zinc material during the charging/discharging process. The morphology and phase composition of the DFs on the positive electrode are the same as their original ones (Figure S14B,D, Supporting Information).

To verify the suitability of this zinc-ion SC as an energy supplier for practical applications, two stand-alone and portable SC demonstrators were designed and fabricated. A light emitting diode (LED) array composed of 16 green LED lamps is arranged in "LOT," which is the abbreviation of our group name in German ("Lehrstuhl für Oberflächen-und Werkstofftechnologie"). When two SCs are connected in series, the LED array can be lighted for more than 70 s (Figure 2F and Clip S1, Supporting Information). In fact, the total mass of positive electrode and negative electrode is only 1.6 mg. The insets in Figure 2F show three states of these LEDs: lamp-off during the charging of the SCs (left), lamp-on just after finishing charging (middle) and lamp-on after a long discharging process (right). The high brightness of the lamp array is indicative of the high power density of this demonstrator device. It is also capable to power this LED array for a long period of time, which hints at its high energy density. The recorded voltage–time curve is stable and reproducible in the successive charging/discharging cycles. If only one zinc-ion SC is applied, a timer can be powered for 15 min (Figure S15 and Clip S2, Supporting Information), further confirming the high energy density of this zinc-ion SC. Consequently, this zinc-ion SC can be stably and reproducibly operated in aqueous solutions. It is thus capable and suitable for practical applications.

To explore the application as a power supply for flexible electronics, the flexibility of such SCs was further evaluated. For these tests, $ZnSO_4$-filled gelatin was employed to host the DFs. Gelatin was selected because of its high solubility of inorganic salts, its environmental friendliness, and its abundance in nature.[22] The as-fabricated SC is easily bent. **Figure 3**A shows images of such experiments with bending angles from the flat configuration to U-shaped bending with a tip radius of around 5 mm. No obvious changes of the CVs are observed when the SC is bent at different angles (Figure 3B) indicating an excellent flexibility of the SCs. Notice that the CVs in Figure 2A are different from those shown in Figure 3B, which is probably due to the changed electrolytes and procedures to assemble these SCs. For example, the conductivity and ion transferring in the gel electrolyte (Figure 3B) are weaker than those in an aqueous electrolyte (Figure 2A). Moreover, the effect of oxygen that is generated from the in situ electrodeposition of zinc nanosheets has little effect on the recorded CVs in the gel electrolyte (Figure 3B), when compared with that in an aqueous electrolyte (Figure 2A). This is because the SC in an aqueous electrolyte was first assembled, followed by the in situ electrodeposition of zinc nanosheets. Differently, the SC in the gel electrolyte was assembled with two DFs sealed in the gel electrolyte. One DF electrode was already coated with zinc nanosheets. Namely, the additional discharging capacitance from oxygen reduction reaction on the DFs does not significantly contribute in the gel electrolyte. Furthermore, the recorded GCD curves are nearly unchanged under all bending conditions (Figure 3C), attesting their superior flexibility. Remarkably, the change of its capacitance is less than 2.43% even after 1000 bending cycles with a bend angle of 60°. Therefore, this diamond zinc-ion SC features excellent durability and superior flexibility. Therefore, such SCs with outperforming electrical performance and flexibility are potential candidate as a power supply for flexible and wearable electronics. Obviously, fabric or woven tests of DFs are required, since these tests will deliver more useful information about the flexible properties of the DFs, which are much important for the practical applications, such as wearable and intelligent electronics.

3. Conclusion

Diamond fibers with fibrous core/shell structure, synthesized by overgrowing carbon fibers with a thin boron-doped diamond layer by chemical vapor deposition, feature the characteristics of both the carbon fibers and the diamond layer. Novel fiber-based zinc-ion supercapacitors have been developed utilizing these flexible DFs as the positive electrode and zinc nanosheet coated DFs as the negative electrode. Those possess outperforming gravimetric and volumetric energy and power densities in conjunction with excellent mechanical flexibility and long-term stability. Its performance is superior to most of the previously reported supercapacitors and batteries. Therefore, this diamond zinc-ion supercapacitor is a new and promising

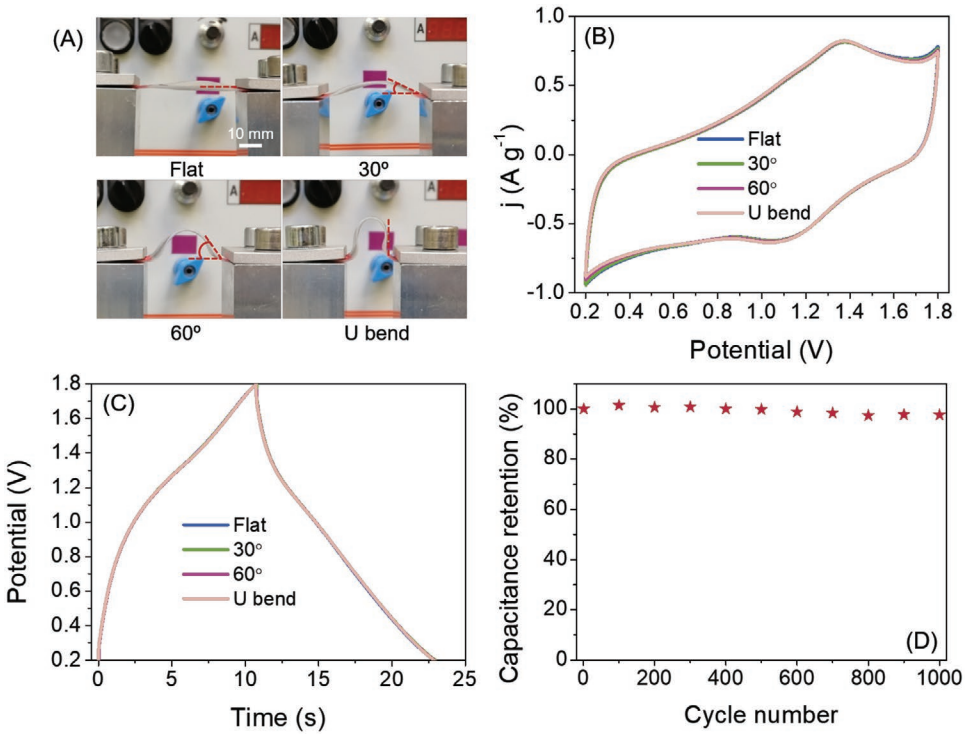

Figure 3. Test of mechanical flexibility of diamond zinc-ion SCs: A) photographs of the SCs at different bending stages, B) CVs and C) GCD curves of the SCs bent with different bending angles, D) Capacitance retention during the periodic bending test (up to 60°) for 1000 times.

candidate for use as an energy supply system for flexible and wearable electronics. The proposed strategies are universally applicable to the design and synthesis of different kinds of flexible electrodes, further facilitating the exploration of applications for these flexible electrodes in the energy and electronics fields.

4. Experimental Section

The synthesis of flexible DFs and the fabrication of zinc-ion SCs from DFs are schematically illustrated in **Figure 4**.

Synthesis of Flexible DFs: In step 1, CF bundles were sputter coated with a titanium (Ti) layer using an RF (13.56 MHz) magnetron sputtering method. A Ti metal (99.99% pure) (4 in. in diameter and 5 mm in thickness) target was sputtered in an Ar (99.999% pure) atmosphere. Sputtering parameters, including background pressure, working pressure, Ar flow rate, RF power, sputtering time and substrate temperature are listed in Table S2 in the Supporting Information. In order to make sure the surface of CFs was fully coated, they were sputter coated twice (the front and back side). This coating prevented the CFs from being etched by the H_2 plasma during the CVD growth process of the BDD layer. Subsequently, the Ti-covered CFs were immersed into a diamond colloid dispersion (New Metals & Chemicals Corporation, Japan) and placed in an ultrasonic bath for 3 min. They were subsequently rinsed in distilled water and dried with N_2 gas. In step 2, BDD thin films were deposited in a microwave plasma enhanced chemical vapor deposition reactor (MWCVD, ASTeX 5000W A5000i model). Under different growth conditions, three diamond fiber samples (named as DF-1, DF-2, and DF-3) were grown. The deposition parameters of this process including the flow rate ratio of H_2 to

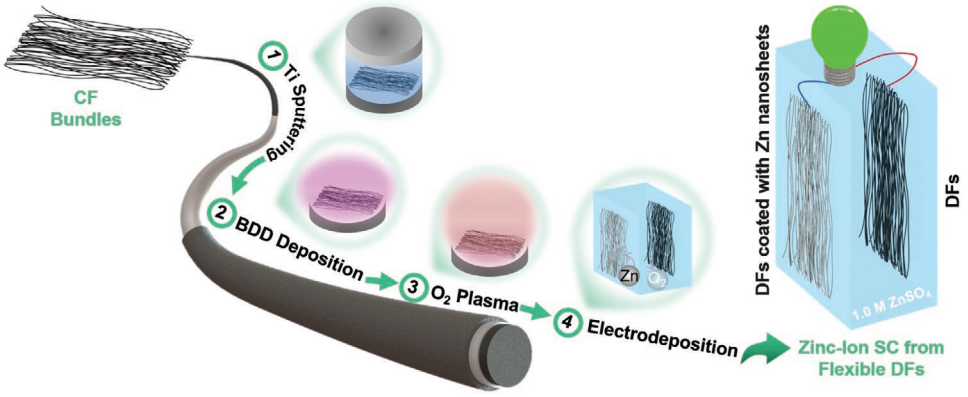

Figure 4. Schematic illustration of the synthesis of flexible DFs and the fabrication of zinc-ion SCs.

CH_4, trimethylborane (TMB), microwave power, working pressure, deposition time, and substrate temperature are listed in Table S1 in the Supporting Information. In step 3, the as-grown DFs were treated by an O_2 plasma (exposure time 2 min, RF power 50 W, gas mixture Ar/O_2 of 50%/50% with flow rate of 15 sccm). Such a treatment led to an increased hydrophilicity (or wettability) of the DFs. These treated DFs were finally utilized in the electrochemical measurements. In step 4, the in situ electrodeposition of zinc nanosheets onto DFs was conducted by the use of linear sweep voltammetry. A three-electrode configuration was used with one FD electrode for Zn deposition (counter electrode) and the other one as reference and working electrode. The potential was scanned in a range of 3.0 to 2.0 V at a scanning rate of 50 mV s^{-1}. The scanning cycle was repeated three times in a solution of 1.0 M $ZnSO_4$. In this process, the zinc ions in the solution were reduced to zinc metal and were deposited onto the DF electrode in the form of metallic nanosheets while oxygen evolution occurred at the other DF electrode.

The morphology of the different DFs was examined using FESEM (Zeiss Ultra 55) and STEM (FEI Talos F200X). The presented FFT was calculated by summing individual FFTs from three HRTEM images acquired at different positions. Owing to the small number of TiC crystallites within the interlayer, this was done to obtain better statistics for further structural analyses. An integrated EDX (Thermo Scientific) was used to do the quantitative element determination of used films during SEM imaging at an acceleration voltage of 15 kV. XRD patterns of the DFs were recorded with an XRD 3000 PTS diffractometer (PANalytical Empyrean) with a Cu Kα radiation source (λ = 1.54 Å). The XPS were collected using Al Kα radiation with a power of 200 W (s-probe ESCA SSX-100s, Surface Science Instruments). Related Raman spectra were recorded using an inVia Raman microscope (RENISHAW). The mapping of doped boron atoms in the BDD films was conducted by time-of-flight secondary ion mass spectrometry (ToF-SIMS IV, ION-TOF GmbH, Germany). The bombardment of the surface was done with a 25 keV Bi^+ primary ion beam on a raster area of 300 × 300 μm^2. For SIMS measurements, BDD film and undoped diamond film were deposited on Si wafer using the deposition parameters of DF-3 with and without TMB, respectively.

Fabrication of Zinc-Ion SCs from Flexible DFs: The zinc-ion SCs were constructed using DFs as the positive electrode and zinc nanosheet coated DFs as the negative electrode (fabricated in step 4). Two capacitor electrodes were mounted between two pieces of acrylic glass sample inserts. A 50 µm thick membrane (Nafion NRE-212) was fixed (or screwed) between the two electrodes. Final zinc-ion SCs were constructed by inserting these electrodes in an electrolytic cell and adding 1.0 M $ZnSO_4$ aqueous solution to the active region. No additional electrolytes or electrodes were needed during the formation of the negative capacitor electrode and the construction of this zinc-ion SC.

The electrochemical performance of the CFs and DFs was evaluated at ambient temperature using CV, the GCD method, and EIS. A CHI 660E electrochemical analyzer (Shanghai Chenhua Inc., China) with either three- or two-electrode configuration was utilized. In the three-electrode system, as-prepared DF electrodes, a Pt wire, and an Ag/AgCl electrode acted as the working, counter, and reference electrodes, respectively. The electrolytes used included 1.0 M $ZnSO_4$, 1.0 M Na_2SO_4, and 1.0 M Na_2SO_4 containing 0.05 M $K_3Fe(CN)_6/K_4Fe(CN)_6$. The CVs were obtained in these aqueous solutions at different scan rates. The Nyquist plots were recorded at open circuit potentials within the frequency range of 100 kHz to 0.01 Hz. All current densities were normalized the mass of the working electrode.

For the performance evaluation of the as-fabricated zinc-ion SCs, the CVs at different scan rates and the GCD curves at different current densities were obtained in a 1.0 M $ZnSO_4$ aqueous solution. The energy densities (E, Wh kg^{-1} or Wh L^{-1}), and power densities (P, W kg^{-1} or W L^{-1}) of the zinc-ion SCs were calculated using the active masses and/or volumes of the two capacitor electrodes.[4e,23] The GCD curves of the zinc-ion DF-SC after the removal of the dissolved oxygen was also recorded in 1.0 M $ZnSO_4$ aqueous solution. The dissolved oxygen was removed through purging nitrogen gas for at least 10 min prior to the recording of these GCD curves.

To test the mechanical flexibility of the as-fabricated zinc-ion SCs, bending tests were conducted using two electrodes sealed in a gel. In the first step, the gel was prepared by adding 2 g of gelatin at room temperature into 15 mL of 1.0 M $ZnSO_4$ aqueous solution, followed by stirring at 80 °C for 2 h. In the second step, the active region of one electrode was covered with this gel on a silicone film, where a Cu wire was connected to the ends of the fibers. Subsequently, the second electrode was placed on top and covered by this gel, thereby sealing the DF capacitor electrodes. The CVs, at a scanning rate of 100 mV s^{-1}, and the GCD curves, at a current density of 1000 mA g^{-1}, were measured when the sample was bent at different angles (e.g., flat, 30°, 60°, and U bend).

Flexible Diamond Zinc-Ion SC Demonstrators: Two demonstrator devices were constructed to I) light an array of 16 green light emitting diodes (LEDs, with a working voltage of 2.3 V) and II) to run a timer (with a working voltage of 1.5 V). In the first example, two zinc-ion SCs were combined in series. In the second one, only one zinc-ion SC was used. The design of the two demonstrator devices was similar to the previously reported SC demonstrator,[4d] for which the electrical circuit diagram is shown in Figure S16 in the Supporting Information. A single-board microcontroller (Arduino UNO) was programmed to automatically control the charging/discharging processes of the demonstrator devices. Briefly, when switch 1 was closed, the device was charged by a universal serial bus (USB) connector. Namely, the charging process starts. The function of the resistor was to adjust the charging current in the circuit. When the measured potential reached the preset value, switch 1 was opened while switch 2 was closed triggering the discharging process. When the measured potential was lower than the preset value in the course of the discharging process, switch 2 was opened and switch 1 was closed. Namely, the device started to repeatedly charge. For example, the demonstrator device used to light the LED array was automatically charged when the voltage came below 1.9 V. The discharging process was automatically started when the voltage exceeded 3.6 V. For the demonstrator to power the timer, the voltage limits were set to 0.9 and 1.8 V for its charging and discharging initiation, respectively. To examine the stability and reproducibility of the charging/discharging processes of these demonstrator devices, their voltage variation was recorded as a function of the charging/discharging time.

Supporting Information

Supporting Information is available from the Wiley Online Library or from the author.

Acknowledgements

The China Scholarship Council is thanked for giving the Ph.D. student stipend to Z.J. (No. 201609150011). Part of this work was performed at the Micro- and Nanoanalytics Facility (MNaF) of the University of Siegen. The authors acknowledge Markus Hartmann (Institute of Material systems for lightweight vehicle construction, University of Siegen, Germany), who kindly provided the XRD spectra of the samples. Ulrike Koch (the Laboratory for Analytical Chemistry, University of Siegen, Germany) is acknowledged for providing the SIMS measurements of the diamond samples. The carbon fibers were provided by Carbon-Werke Weißgerber GmbH & Co. KG (Wallerstein, Germany).

Open access funding enabled and organized by Projekt DEAL.

Conflict of Interest

The authors declare no conflict of interest.

Keywords

boron-doped diamonds, energy densities, flexible electronics, flexible supercapacitors, zinc-ion supercapacitors

Received: July 6, 2020
Revised: August 24, 2020
Published online:

[1] a) C. Zhong, Y. Deng, W. Hu, J. Qiao, L. Zhang, J. Zhang, *Chem. Soc. Rev.* **2015**, *44*, 7484; b) J. Wang, S. Li, F. Yi, Y. Zi, J. Lin, X. Wang, Y. Xu, Z. L. Wang, *Nat. Commun.* **2016**, *7*, 12744; c) W. Liu, M.-S. Song, B. Kong, Y. Cui, *Adv. Mater.* **2017**, *29*, 1603436; d) H. Sun, S. Xie, Y. Li, Y. Jiang, X. Sun, B. Wang, H. Peng, *Adv. Mater.* **2016**, *28*, 8431.

[2] a) L. Liu, Y. Yu, C. Yan, K. Li, Z. Zheng, *Nat. Commun.* **2015**, *6*, 7260; b) S. Zhai, H. E. Karahan, C. Wang, Z. Pei, L. Wei, Y. Chen, *Adv. Mater.* **2020**, *32*, 1902387; c) W. Jiang, S. Zhai, Q. Qian, Y. Yuan, H. E. Karahan, L. Wei, K. Goh, A. K. Ng, J. Wei, Y. Chen, *Energy Environ. Sci.* **2016**, *9*, 611.

[3] a) X. Wang, B. Liu, R. Liu, Q. Wang, X. Hou, D. Chen, R. Wang, G. Shen, *Angew. Chem., Int. Ed.* **2014**, *53*, 1849; b) F. Mo, G. Liang, Z. Huang, H. Li, D. Wang, C. Zhi, *Adv. Mater.* **2020**, *32*, 1902151; c) X. Chen, H. Lin, J. Deng, Y. Zhang, X. Sun, P. Chen, X. Fang, Z. Zhang, G. Guan, H. Peng, *Adv. Mater.* **2014**, *26*, 8126.

[4] a) N. Yang, S. Yu, J. V. Macpherson, Y. Einaga, H. Zhao, G. Zhao, G. M. Swain, X. Jiang, *Chem. Soc. Rev.* **2019**, *48*, 157; b) S. Yu, K. J. Sankaran, S. Korneychuk, J. Verbeeck, K. Haenen, X. Jiang, N. Yang, *Nanoscale* **2019**, *11*, 17939; c) J. Xu, N. Yang, S. Heuser, S. Yu, A. Schulte, H. Schönherr, X. Jiang, *Adv. Energy Mater.* **2019**, *9*, 1803623; d) S. Yu, N. Yang, M. Vogel, S. Mandal, O. A. Williams, S. Jiang, H. Schönherr, B. Yang, X. Jiang, *Adv. Energy Mater.* **2018**, *8*, 1870054; e) S. Yu, N. Yang, H. Zhuang, S. Mandal, O. A. Williams, B. Yang, N. Huang, X. Jiang, *J. Mater. Chem. A* **2017**, *5*, 1778; f) N. Yang, in *Novel Aspects of Diamond: From Growth to Applications*, (Eds: N. Yang), Springer International Publishing, Switzerland **2019**, pp. 223–256.

[5] F. Gao, C. E. Nebel, *ACS Appl. Mater. Interfaces* **2016**, *8*, 28244.

[6] a) N. Choudhary, C. Li, J. Moore, N. Nagaiah, L. Zhai, Y. Jung, J. Thomas, *Adv. Mater.* **2017**, *29*, 1605336; b) F. Zhang, T. Zhang, X. Yang, L. Zhang, K. Leng, Y. Huang, Y. Chen, *Energy Environ. Sci.* **2013**, *6*, 1623; c) H. Wang, Y. Zhang, H. Ang, Y. Zhang, H. T. Tan, Y. Zhang, Y. Guo, J. B. Franklin, X. L. Wu, M. Srinivasan, H. J. Fan, Q. Yan, *Adv. Funct. Mater.* **2016**, *26*, 3082.

[7] a) F. Wang, X. Wang, Z. Chang, X. Wu, X. Liu, L. Fu, Y. Zhu, Y. Wu, W. Huang, *Adv. Mater.* **2015**, *27*, 6962; b) L. Fan, K. Lin, J. Wang, R. Ma, B. Lu, *Adv. Mater.* **2018**, *30*, 1800804; c) L. Dong, X. Ma, Y. Li, L. Zhao, W. Liu, J. Cheng, C. Xu, B. Li, Q.-H. Yang, F. Kang, *Energy Storage Mater.* **2018**, *13*, 96; d) V. Aravindan, J. Gnanaraj, Y.-S. Lee, S. Madhavi, *Chem. Rev.* **2014**, *114*, 11619.

[8] a) H. Wang, M. Wang, Y. Tang, *Energy Storage Mater.* **2018**, *13*, 1; b) X. Wang, J. Gao, Z. Cheng, N. Chen, L. Qu, *Angew. Chem., Int. Ed.* **2016**, *55*, 14643.

[9] a) J. Shi, S. Wang, X. Chen, Z. Chen, X. Du, T. Ni, Q. Wang, L. Ruan, W. Zeng, Z. Huang, *Adv. Energy Mater.* **2019**, *9*, 1901957; b) Q. Wang, S. Wang, X. Guo, L. Ruan, N. Wei, Y. Ma, J Li, M. Wang, W. Li, W. Zeng, *Adv. Electron. Mater.* **2019**, *5*, 1900537.

[10] a) S. Ozkan, H. Ghanem, S. Mohajernia, S. Hejazi, T. Fromm, R. Borchardt, S. Rosiwal, P. Schmuki, *ChemElectroChem* **2019**, *6*, 4545; b) S. Kono, T. Teraji, H. Kodama, K. Ichikawa, S. Ohnishi, A. Sawabe, *Diamond Relat. Mater.* **2015**, *60*, 117.

[11] a) X. J. Li, Y. S. Li, L. L. He, Q. Yang, A. Hirose, *Mater. Chem. Phys.* **2014**, *143*, 647; b) S. J. Askari, G. C. Chen, F. X. Lu, *Mater. Res. Bull.* **2008**, *43*, 1086.

[12] a) R. J. Zhang, S. T. Lee, Y. W. Lam, *Diamond Relat. Mater.* **1996**, *5*, 1288; b) Y. Feng, J. Lv, J. Liu, N. Gao, H. Peng, Y. Chen, *Appl. Surf. Sci.* **2011**, *257*, 3433.

[13] a) S. Ghodbane, D. Ballutaud, F. Omnès, C. Agnès, *Diamond Relat. Mater.* **2010**, *19*, 630; b) C. H. Goeting, F. Marken, A. Gutiérrez-Sosa, R. G. Compton, J. S. Foord, *Diamond Relat. Mater.* **2000**, *9*, 390.

[14] a) S. Ferro, M. Dal Colle, A. De Battisti, *Carbon* **2005**, *43*, 1191; b) J. Fan, H. Shi, H. Xiao, G. Zhao, *ACS Appl. Mater. Interfaces* **2016**, *8*, 28306.

[15] E. Brillas, C. A. Martínez-Huitle, in *Synthetic Diamond Films: Preparation, Electrochemistry, Characterization and Applications*, John Wiley & Sons, Inc., Hoboken, NJ **2011**, pp. 155–180.

[16] G. Sun, H. Yang, G. Zhang, J. Gao, X. Jin, Y. Zhao, L. Jiang, L. Qu, *Energy Environ. Sci.* **2018**, *11*, 3367.

[17] a) G. M. Zhou, D. W. Wang, L. C. Yin, N. Li, F. Li, H. M. Cheng, *ACS Nano* **2012**, *6*, 3214; b) X. Y. Shan, Y. Wang, D. W. Wang, F. Li, H. M. Cheng, *Adv. Energy Mater.* **2016**, *6*, 1502064.

[18] R. Wang, J. Lang, P. Zhang, Z. Lin, X. Yan, *Adv. Funct. Mater.* **2015**, *25*, 2270.

[19] N. Suo, H. Huang, A. Wu, G. Cao, X. Hou, G. Zhang, *Appl. Surf. Sci.* **2018**, *439*, 329.

[20] a) Z. Yang, J. Deng, X. Chen, J. Ren, H. Peng, *Angew. Chem., Int. Ed.* **2013**, *52*, 13453; b) J. Yu, W. Lu, J. P. Smith, K. S. Booksh, L. Meng, Y. Huang, Q. Li, J.-H. Byun, Y. Oh, Y. Yan, T.-W. Chou, *Adv. Energy Mater.* **2017**, *7*, 1600976; c) N. Yu, H. Yin, W. Zhang, Y. Liu, Z. Tang, M.-Q. Zhu, *Adv. Energy Mater.* **2016**, *6*, 1501458; d) T. Qin, S. Peng, J. Hao, Y. Wen, Z. Wang, X. Wang, D. He, J. Zhang, J. Hou, G. Cao, *Adv. Energy Mater.* **2017**, *7*, 1700409.

[21] a) P. Simon, Y. Gogotsi, *Nat. Mater.* **2008**, *7*, 845; b) B. Evanko, S. W. Boettcher, S. J. Yoo, G. D. Stucky, *ACS Energy Lett.* **2017**, *2*, 2581.

[22] a) N. A. Choudhury, S. Sampath, A. K. Shukla, *J. Electrochem. Soc.* **2008**, *155*, A74; b) X. Liu, P. X. Ma, *Biomaterials* **2009**, *30*, 4094; c) H. Li, C. Han, Y. Huang, Y. Huang, M. Zhu, Z. Pei, Q. Xue, Z. Wang, Z. Liu, Z. Tang, Y. Wang, F. Kang, B. Li, C. Zhi, *Energy Environ. Sci.* **2018**, *11*, 941.

[23] F. Béguin, V. Presser, A. Balducci, E. Frackowiak, *Adv. Mater.* **2014**, *26*, 2219.